ORIGINAL PAPER

Seismic hazard analysis and local site effect of the 2017 M_w 7.3 Sarpol-e Zahab, Iran, earthquake

Hamid Zafarani[1] · Yaser Jafarian[1] · Alireza Eskandarinejad[2] · Ali Lashgari[3] · Mohammad Reza Soghrat[1] · Hassan Sharafi[4] · Masoud Afraz-e Haji-Saraei[5]

Abstract

A strong earthquake occurred on November 12, 2017, in Sarpol-e Zahab city, western Iran, with the moment magnitude (M_w) of 7.3 and a focal depth of 18 km. The maximum horizontal peak ground acceleration of 0.69 g was recorded at the Sarpol-e Zahab station. Significant damages were observed in frame and masonry buildings, while the damage distribution was non-uniform throughout this small city. The preliminary site reconnaissance revealed that numerous engineering structures collapsed or considerably damaged in some regions, contrary with those non-structural masonry buildings in other regions which remained intact during earthquake. This paper represents a preliminary reconnaissance report prepared through the site visit done by the authors, a few days following the earthquake occurrence. Then, the data recorded by the strong ground motion stations in the affected city and the surrounding regions together with the geotechnical data gathered from the available boreholes in Sarpol-e Zahab are incorporated for probabilistic seismic hazard and local site effect analyses. The observed response spectra at two stations and distance-dependency of ground acceleration are compared with those predicted by some attenuation models. The results of probabilistic seismic hazard analysis in the return periods of 475 and 2475 years are compared with the observed ground response and the design spectra recommended by the Iranian seismic code (for site classes Types I and II). Several geotechnical boreholes from the previous works in the affected area were analyzed through the equivalent-linear site response approach in order to obtain the seismic response at the soil surface. The results are then compared with the code design spectra for the site classes of Types III and IV. It is demonstrated that the calculated response spectra are generally larger than those recommended by the Iranian seismic code, especially for the 4–7 stories buildings.

Keywords Sarpol-e Zahab earthquake · Seismic hazard · Site effect · Uniform hazard spectra · ground motion prediction equations

✉ Yaser Jafarian
   yjafarianm@iiees.ac.ir

Extended author information available on the last page of the article

1 Introduction

On Sunday, November 12, 2017, at 21:48:16 local time, a strong earthquake occurred in the border region between Iran and Iraq in Kermanshah province in the vicinity of Sarpol-e Zahab city. The epicenter coordinates of the earthquake with moment magnitude (M_w) of 7.3 and a focal depth of 18.1 km were reported at 34.77 N and 45.76 E by the Iranian Seismological Center (IRSC, available at https://irsc.ut.ac.ir/). The locations of earthquake epicenter and the recording stations are shown in Fig. 1. This earthquake was the largest seismic event after the M7.4, 1909 AD Silakhor earthquake near the Borujerd city in the Zagros region (Farzanegan et al. 2017). The Sarpol-e Zahab earthquake triggered several landslides and extensive building damages resulting more than 600 deaths and 7000 homeless. The earthquake was apparently felt by people living in the cities located at the distances of several hundred kilometers such as Tabriz and Arak. Compared with the other cities around the epicenter, majority of the structural damages occurred in Sarpol-e Zahab and its neighbor villages. The maximum horizontal peak ground acceleration (PGA) of
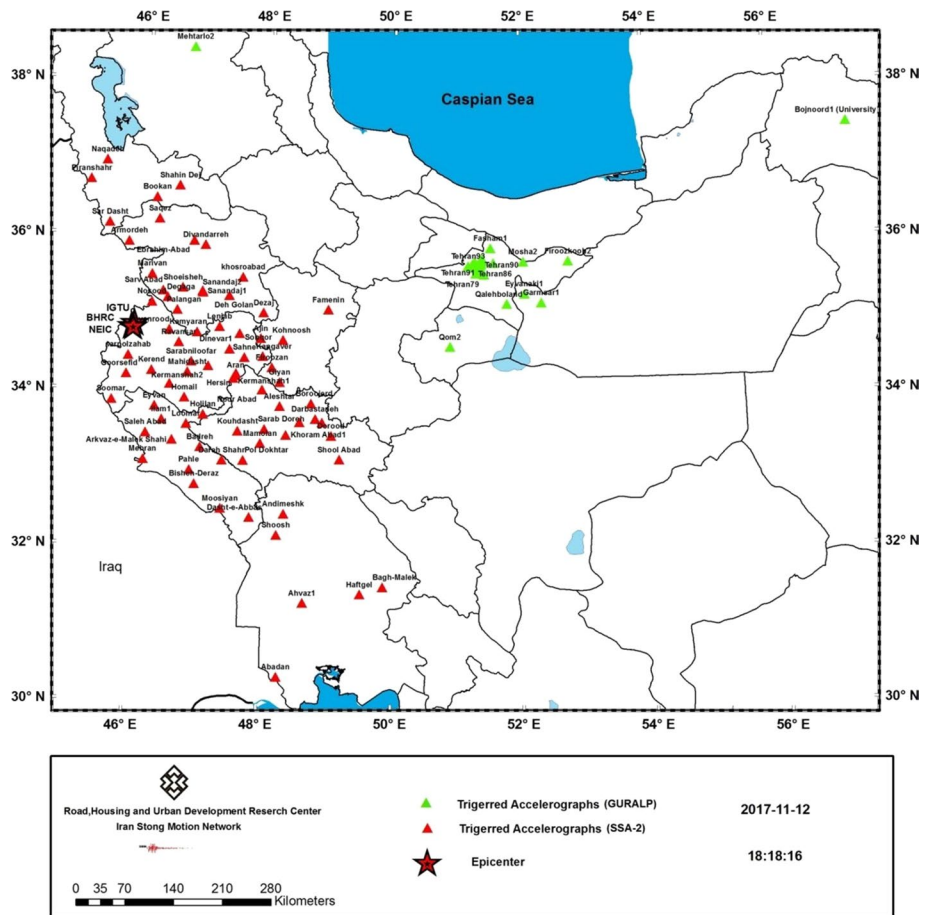

Fig. 1 Map of the epicenter and the recording stations of the Sarpol-e Zahab earthquake (Farzanegan et al., 2017)

0.69 g was recorded at the Sarpol-e Zahab station. However, the damage pattern was not uniform in different parts of the city.

This paper presents results of field observation and also various analyses in four general parts: First, a summary of the reconnaissance report is provided to describe the types of damages in Sarpol-e Zahab during the earthquake. Second, the corrected earthquake records are presented in order to be utilized in the analyses. Third, results of the probabilistic seismic hazard analysis (PSHA) for a reference site are presented to characterize the earthquake ground shaking and to compare the results with the observed ground motions and the standard design spectra of Iran (standard 2800, 2014, hereafter, BHRC14). Finally, results of the local site effect analysis are presented for a selected site of Sarpol-e Zahab by the available geotechnical and geophysical data.

2 Preliminary reconnaissance report

Widespread damages were observed throughout the west of the Kermanshah province including Sarpol-e Zahab, Eslamabad-e Gharb, Kerend-e Gharb, Ezgeleh, and Salas-e Babajani cities during the Sarpol-e Zahab earthquake in the Kermanshah province, Iran. The maximum value of peak ground acceleration (PGA) was recorded at the Sarpol-e Zahab station at an epicentral distance of 35 km. The peak horizontal and vertical accelerations at this station were 0.69 g and 0.33 g, respectively. Significant damages of non-structural elements of building mainly the infill walls occurred in the Maskan-Mehr residential complex which has built in 2012 with 576 units. Buildings collapse in the regions around the Maskan-Mehr buildings was clearly more than the other sides of the city. The geotechnical and structural damages observed throughout the Sarpol-e Zahab city are summarized as below.

2.1 Geotechnical aspects

Geotechnical damages, mainly ground displacement, were observed throughout the city especially in the alluvial areas near the river. Evidences of embankment failure occurred in the neighborhood of Maskan-Mehr as shown in Fig. 2a. Figure 2b shows the catastrophic collapse of a steel structure in the Fouladi neighborhood which led to 38 deaths. This structure was located near the edge of slope which may be visible in Fig. 2b. The slope was constructed by loose fill materials. The field surveys indicate that there are several construction problems in joints and welds of the structure which caused collapse of the structure; however, the structure probably was designed improperly.

2.2 Structural aspects

Figure 3 illustrates some damaged structures superimposed on the damage density map of the Sarpol-e Zahab city. The map was produced by the UNITAR-UNOSAT analysis. The damage density map indicates that the neighborhood of Maskan-Mehr and the area around the Post Office are amongst the most affected zones. The damages suffered by various newly constructed structures were observed by the authors as shown in Fig. 3. Our field investigation generally confirms the UNITAR–UNOSAT analysis for the

Fig. 2 The geotechnical aspect of the Sarpol-e Zahab earthquake **a** failure of soft soil embankment **b** collapse of the structure constructed on the weak ground

potentially damaged structures. The observations indicate that most of the structures (concrete or steel) have been damaged in the beam-column connections. Moreover, the insufficient shear capacity of columns has played a major role in the structural failures. The 7-story reinforced concrete (RC) buildings of the Maskan-Mehr residential complex are shown in the upper left corner of Fig. 3. It is seen that the brick masonry infill walls were completely destroyed, possibly due to lack of lateral restraint in the walls, while the damages in the structural frame were negligible under earthquake. However, the column shear failure was observed in a few cases. This issue reduced the human death due to earthquake in Maskan-Mehr residential complex. A RC-building of Fouladi and Taze Abad neighborhoods is shown in the center left and bottom right corner of Fig. 3, respectively. The RC apartment complex collapsed, possibly due to "short column"
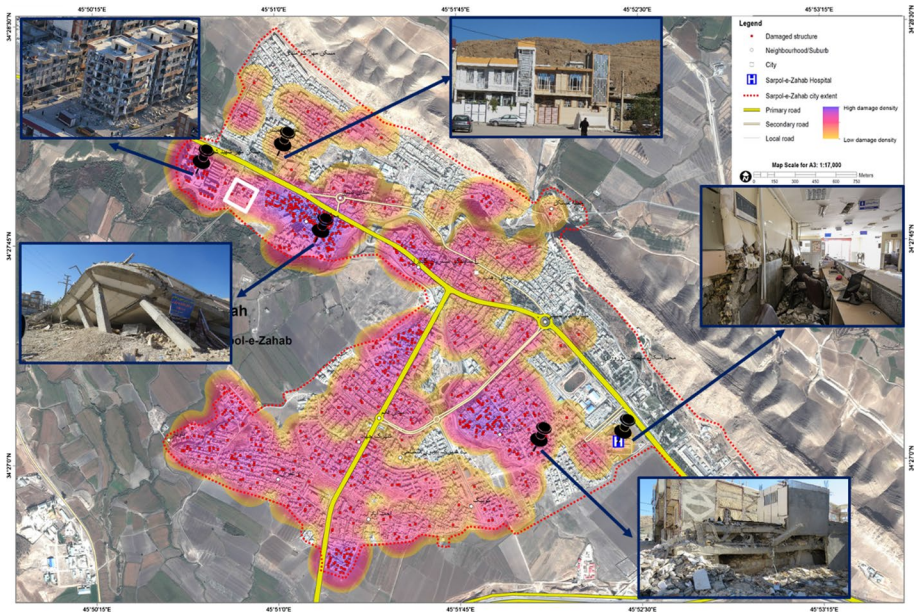
**Fig. 3** The damaged structures and related density map in Sarpol-e Zahab (after UNITAR-UNOSAT)

behavior. Moreover, the stirrup and lap splices of longitudinal rebars were insufficient in the columns.

3 Strong motion records correction

The Sarpol-e Zahab earthquake was recorded by 109 free-field strong motion stations (including SSA-2 and Guralp CMG5TD instruments) as shown in Fig. 1. Due to lower threshold level of CMG-5TD accelerometers, this earthquake is recorded at long distances such as the Bojnourd University station at distance of about 1000 km or the stations in Tehran city with epicentral distances of more than 500 km.

The acceleration time series were provided in raw format by the BHRC (Building and Housing Research Center). Therefore, they must be baseline corrected and proper filtered to eliminate high- and low-frequency noises (Zafarani and Soghrat 2017). Although a classic technique based on the signal-to-noise ratio is usually used to correct the records, in this study, the multi-resolution wavelet analysis was employed to eliminate undesirable noise from the recorded signals (proposed by Ansari et al. 2010). After the correcting procedure, 50 records have been recognized as poor quality records and excluded from the analysis. The maximum recorded PGA is about 0.69 g and 0.33 g for horizontal and vertical components, respectively, in the Sarpol-e Zahab station. The distribution of PGAs of remaining records (59 records) in horizontal (PGA_H) and vertical (PGA_V) components is illustrated in Fig. 4 to show the correlation between the two components. The distribution of PGA versus distance for the horizontal and vertical components is also shown in the figure. Moreover, the epicentral distance of these records and the average shear wave velocity between 0 and 30-m depth (V_{s30}) in each station are plotted in Figs. 5 and 6, respectively.

Fig. 4 The distribution of PGAs (the geometric average) in the recorded stations: horizontal PGA (top), vertical PGA (middle), and correlation between two components (bottom)
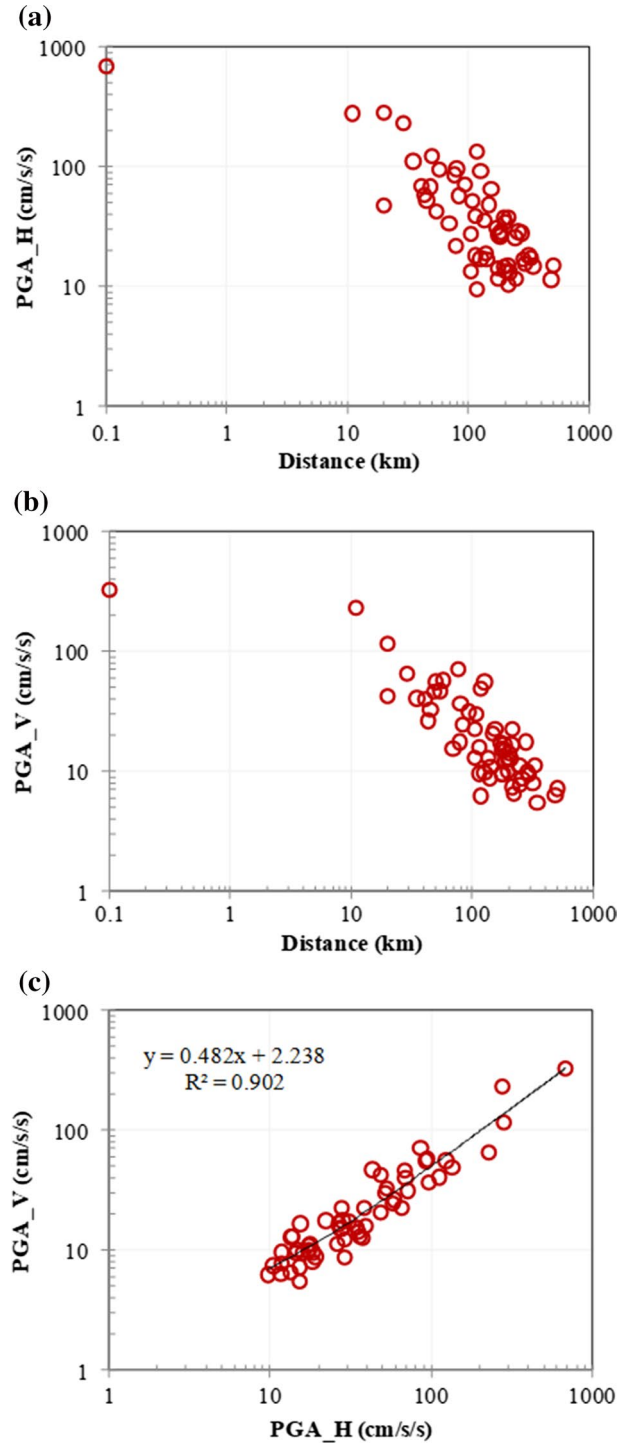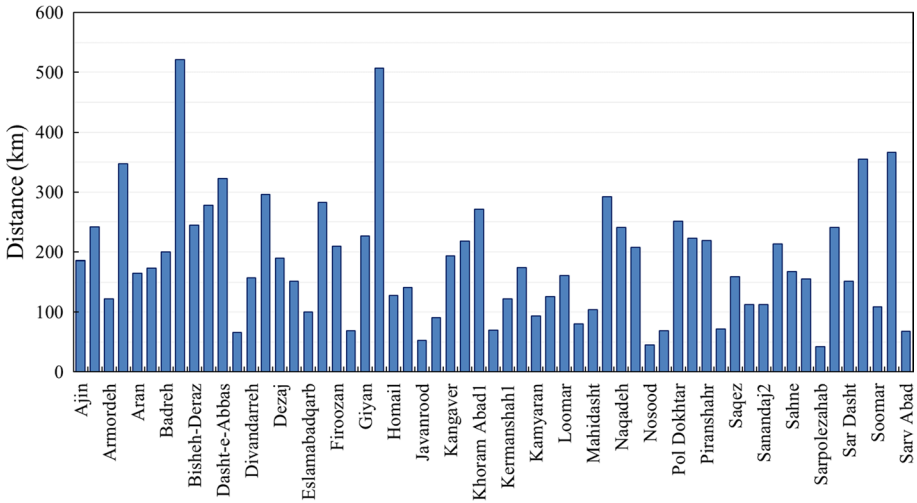
Fig. 5 The distance between the recorded stations and epicenter of earthquake
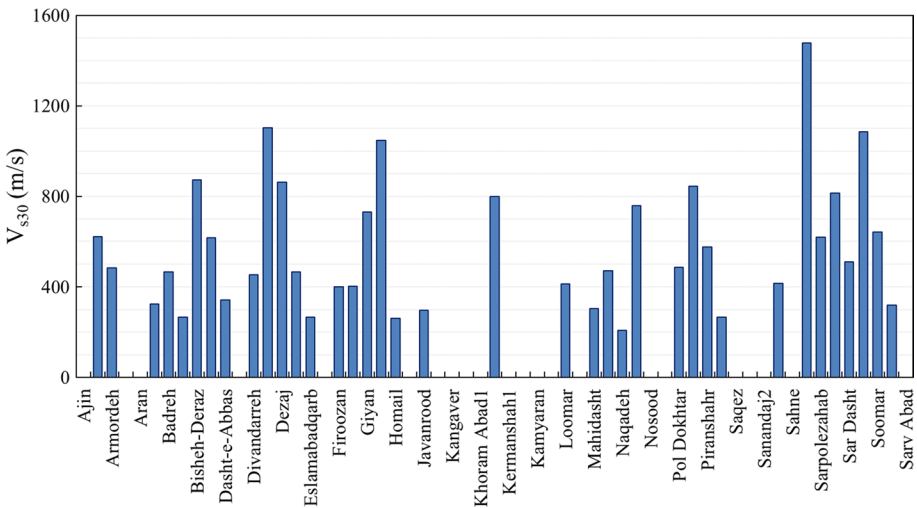

Fig. 6 The V_{s30} distribution in the recorded stations

The observed spectral acceleration (SA) in two stations [including the Sarpol-e Zahab (SPZ) and Kerend (KRD) stations] was compared with the values predicted by five ground motion prediction equations (GMPEs) in Fig. 7. We believe that the GMPEs developed for active shallow crustal tectonic regimes can be applicable to the shallow zones. Therefore, we used the GMPEs developed based on the local, regional, and global data. It is tried to select the latest GMPEs such as Boore et al. (2014), Campbell and Bozorgnia (2014), Abrahamson et al. (2014), Chiou and Youngs (2014), and etc. Moreover, two local GMPEs which are developed based on Iranian database have been used. In addition, the criteria that proposed by Bommer et al. (2010) have been considered in

Fig. 7 Comparison of observed
and predicted spectral accelera-
tions in SPZ and KRD stations.
Obs observed data, *Zea18* Zafa-
rani et al. (2018), *BSSA14* Boore
et al. (2014), *CB14* Campbell
and Bozorgnia (2014), *ASK14*
Abrahamson et al. (2014), *ZS12*
Zafarani and Soghrat (2012)
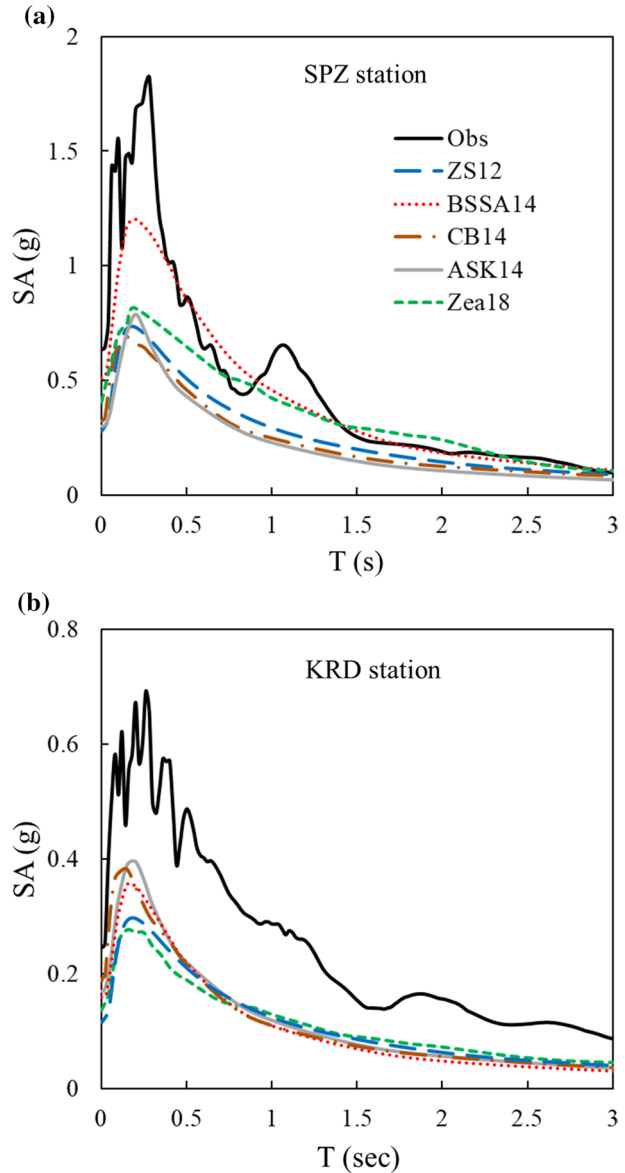
selection of GMPEs. The models proposed by Zafarani et al.(2018), Boore et al.(2014),
Campbell and Bozorgnia (2014), Abrahamson et al. (2014), and Zafarani and Soghrat
(2012) have been chosen for the comparison purpose. Figure 7 shows that the model
proposed by Boore et al. (2014) is compatible with the observed values in the Sarpol-e
Zahab station for periods beyond 0.4 s. The model proposed by Zafarani et al. (2018)
can predict properly in periods more than 0.7 s in the Sarpol-e Zahab station. It is noted
that the observed values in the Kerend station are considerably different from the values
predicted by the GMPE models. The geometric average of horizontal components has
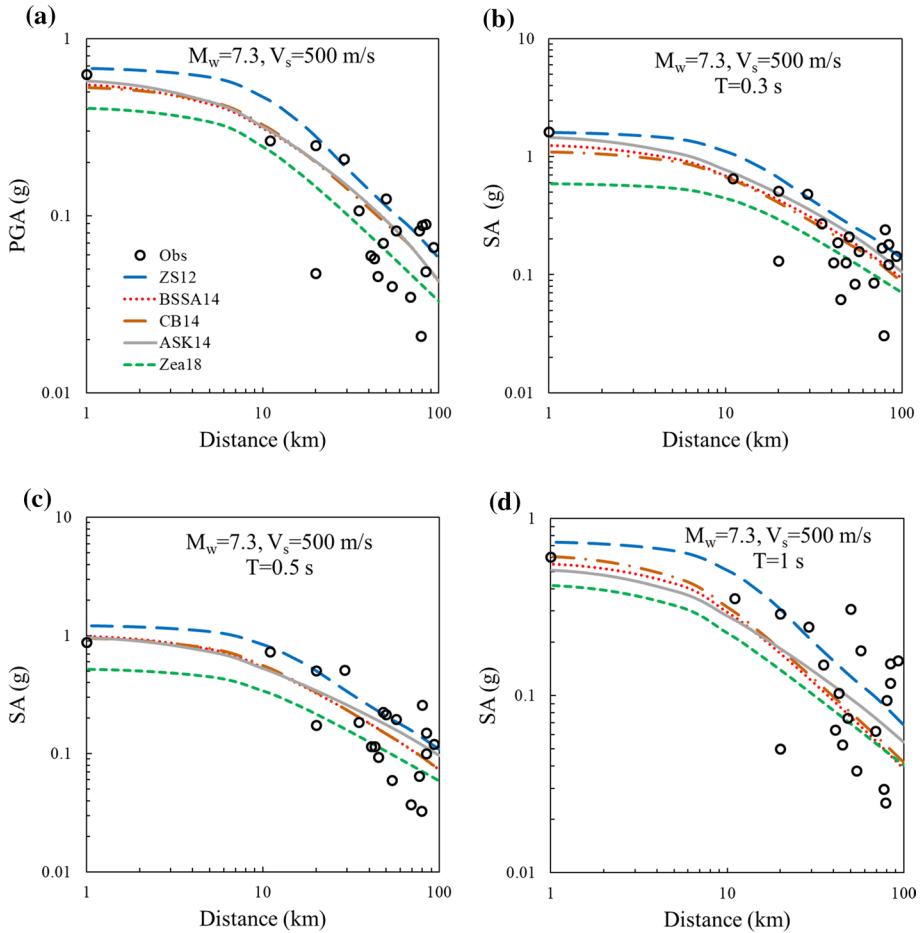
Fig. 8 Comparison of the observed values and predictions of the GMPEs for the geometric average of horizontal components. *Obs* Observed data, *Zea18* Zafarani et al. (2018), *BSSA14* Boore et al. (2014), *CB14* Campbell and Bozorgnia (2014), *ASK14* Abrahamson et al. (2014), *ZS12* Zafarani and Soghrat (2012)

been used in this study. In addition, the V_{s30} is considered 619 and 800 m/s for SPZ and KRD stations, respectively, and GMPEs are adjusted for these different values.

Figure 8 represents the distance dependency of observed PGAs and SAs at periods of 0.3, 0.5, and 1 s. Figure 8a–d is based on the moment magnitude of 7.3 and site class II ($V_{s30} = 500$ m/s). It seems that for short periods, the model proposed by Zafarani et al. (2018) works better than the other models. Figure 8 shows that for long periods, the models proposed by Boore et al. (2014) and Campbell and Bozorgnia (2014) have done a better job for prediction of observed data. There are different quantitatively monitoring to understand the agreement between observed and predicted data. However, in some cases, determination of suitability for the GMPEs has been investigated using a direct comparison between median GMPEs and the observed data (Zafarani and Farhadi 2017). In this study, we used direct comparison between median GMPEs and the observed data.

4 Seismic hazard analysis

First step of a probabilistic seismic hazard analysis (PSHA) includes gathering an earthquake catalog for the given region. Previously, several studies (e.g. Ambraseys and Melville, (2005) Berberian, (1994) Mirzaei et al.(1998) Shahvar et al.(2013) Zare et al.(2014) Khodaverdian et al., (2016) have been carried out to compile the uniform earthquake catalog of Iran and its surroundings. In the current research, an extension of the catalog provided by Khodaverdian et al. (2016) along with the events presented by Zare et al. (2014) was prepared using the data extracted from the IRSC. Since the IRSC reports the modified Nuttli magnitude scale (M_N) for each event, and in order to provide a uniform catalog, M_N values of each event were converted to moment magnitude (M_w) using the following relationship proposed by Shahvar et al. (2013):

$$M_w = 0.834 M_N + 0.932 \qquad (1)$$

The historical earthquakes were collected from different studies such as Zare et al. (2014), Khodaverdian et al. (2016), and Onur et al. (2017). Zare et al. (2014) and Khodaverdian et al. (2016) used a large number of previous researches to identify the historical events as well as the instrumental ones. Onur et al. (2017) gathered a comprehensive earthquake catalog for Iraq and surroundings. The area studied in the present work was located in the neighborhood of eastern part of Iraq. Hence, the catalog collected by Onur et al. (2017) was considered to achieve a complete catalog for the area of interest. The final catalog is shown in Fig. 9.

For the study region, the final catalog contains 3480 instrumental earthquakes (which occurred from 1903 to 2017) and 22 historical earthquakes that occurred from A.D. 859 to A.D. 1880. To separate main shocks from aftershocks and foreshocks, and eliminate any duplicate events, declustering of the events noted above was performed using the windowing algorithm proposed by Gardner and Knopoff (1974); however, alternative window parameter settings proposed more recently by Gruenthal (implemented in the Wiemer's ZMAP package, 2001) were applied. The parameter settings proposed by Gruenthal identify more events as being dependent for lower magnitudes (<M6.5). The Gruenthal and Gardner and knopoff relationships give approximately similar time and distance windows for large events. Finally, 432 clusters of earthquakes were determined and 993 events remained in the declustered catalog (see Fig. 9).

4.1 Seismicity parameters of source zones

By comparing trends of all faults located in the area of interest with spatial distribution of the regional catalog, considering also other important features such as focal mechanism, tectonic regime, and depth of seismic events (Danciu et al., 2018), nine area source zones were determined that are shown in Fig. 10. Each area source represents only a single geological unit or tectonic feature and all of them are active regions in shallow crust (seismicity depth <40 km). These source zones can be divided into two main categories comprising area type zones along the main trend of the Zagros faults (i.e. source zones 1–6) and background-type zones (i.e. source zones 7–9). Based on the Iranian seismotectonic provinces proposed by Mirzaei et al. (1998), it can be said that the source zones 1–7 belong to the Zagros Province. Furthermore, major part of the source zone 8 is located in the Central-East Iran Province. Southwestern part of the study area is approximately situated in Iraq
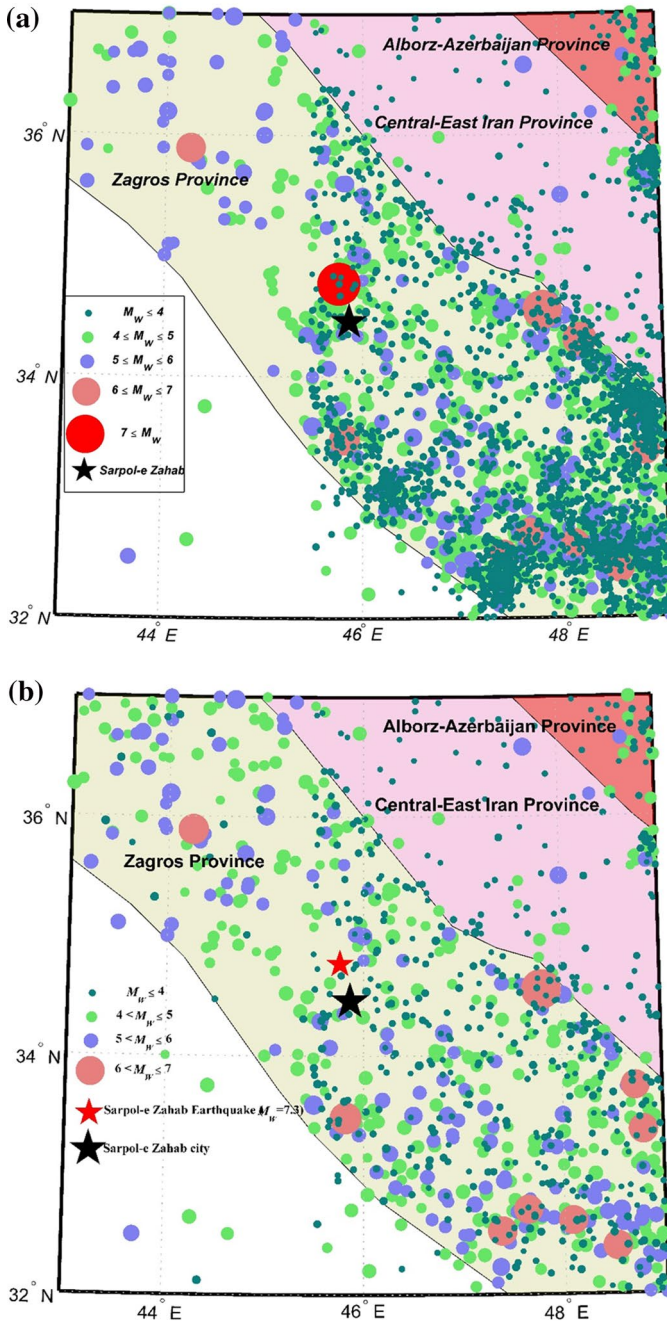
Fig. 9 Epicentral distribution of seismicity in the area of interest, compilation from different sources, **a** original catalog **b** declustered
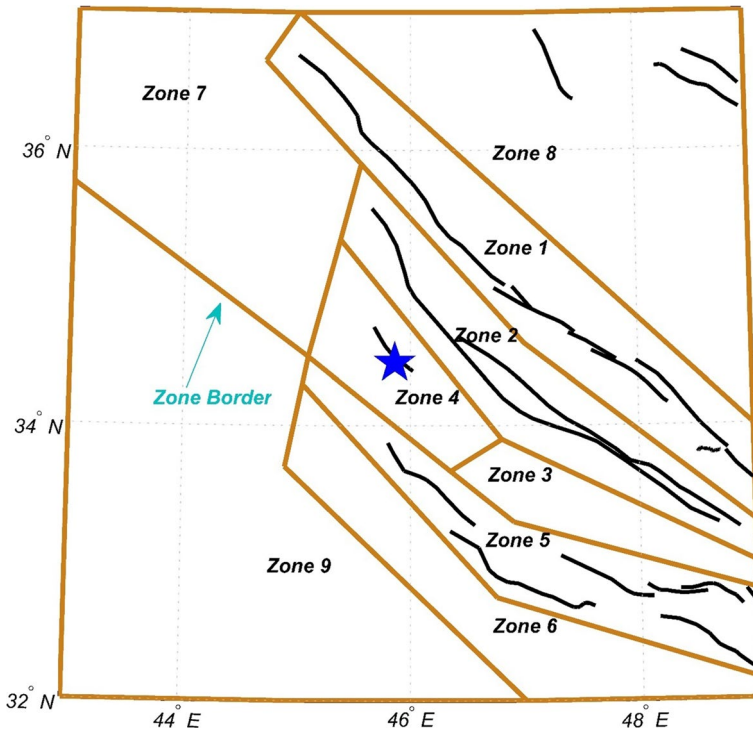
Fig. 10 The seismogenic source model considered in this study

and out of the seismotectonic provinces mentioned above. As seen in Fig. 10, the area zone 4 covers Sarpol-e Zahab city and its proximity.

Completeness magnitude (M_c) should be determined before estimating the seismicity parameters of each source zones. Then, completeness magnitudes and their corresponding time periods were selected from the values proposed by Khodaverdian et al. (2016). It should be noted that M_c was considered equal to 5.0, 4.9, and 3.3 for the time periods of 1900–1964, 1964–1998, and 1998–2017, respectively. Moreover, for different time periods, the completeness magnitude associated with their uncertainties in magnitude (Table 1) was selected based on Khodaverdian et al., (2016).

Time period	Completeness magnitude, M_c	Uncertainty value
< 1918	5.0	0.5
1918–1964	5.0	0.4
1964–1995	4.9	0.3
1995–1998	4.9	0.2
1995–2004	3.3	0.2
2004 <	3.3	0.1

Table 1 Uncertainties in magnitude along with the completeness magnitude, M_c for different time periods (after Khodaverdian et al. 2016)

Table 2 Seismicity parameters of all areal sources

Zone number	m_{min}	λ_{min}(year^{-1})	m_{max}	Uncertainty of m_{max}	β	Uncertainty of β
1	4.5	0.44817	7.5	0.52	2.16	0.13
2	4.5	0.53254	7.5	0.51	1.88	0.17
3	4.5	0.31576	7.5	0.51	1.41	0.21
4	4.5	0.23299	7.5	0.51	1.47	0.29
5	4.5	0.87429	7.5	0.51	1.42	0.13
6	4.5	0.32381	7.5	0.52	1.84	0.15
7	4.5	0.67018	7.5	0.51	1.20	0.14
8	4.5	0.16003	7.9	0.77	2.31	0.20
9	4.5	0.21625	6.5	0.50	1.50	0.26

Table 3 Different GMPEs and their corresponding characteristics

GMPE	Assumed Site condition	Distance metric	Magnitude range
Zafarani and Soghrat (2012)	Rock (V_{S30} > 300 m/s)	1 km ≤ R_{epi} ≤ 200 km	4.4–7.5
Zafarani et al. (2018)	Rock (V_{S30} > 800 m/s)	R_{JB} ≤ 200 km	4.0–7.3
Kale et al. (2015)	V_{S30} = 760 m/s	R_{JB} ≤ 200 km	4.0–8.0
Boore et al. (2014)	V_{S30} = 760 m/s	0 km ≤ R_{JB} ≤ 400 km	3.0–8.5
Idriss (2008)	V_{S30} = 760 m/s	R_{rup} ≤ 200 km	5.0–8.5
Zhao et al. (2006)	V_{S30} > 600 m/s	0.4 km ≤ R_{rup} ≤ 300 km	5.0–9.0
Kanno et al. (2006)	V_{S30} = 750 m/s	1 km ≤ R_{rup} ≤ 400 km	5.5–8.0

Assuming the Poissonian distribution for sequence of earthquake events in the region, and based on the maximum likelihood method proposed by Kijko and Sellevoll (1989, 1992) and Kijko (2004), the MATLAB code HA2 (Kijko 2010) was employed to estimate the seismicity parameters for each source zone. The double-truncated Gutenberg–Richter recurrence model was applied as the frequency–magnitude distribution for each zone as follows.

$$\lambda(m) = \lambda_{min} \frac{e^{-\beta(m-m_{min})} - e^{-\beta(m_{max}-m_{min})}}{1 - e^{-\beta(m_{max}-m_{min})}} \tag{2}$$

where λ denotes the seismicity rate for events with magnitude (m) ≥ minimum magnitude (m_{min}). Other parameters given in Eq. (2) include seismic activity rate corresponding to m_{min} (λ_{min}), maximum magnitude (m_{max}), and regression coefficient (β = bLn10). The lower threshold magnitude, m_{min}, has been chosen on the basis of the minimum magnitude that is capable of causing significant damage and below which there is no engineering interest. m_{min} is usually selected to be between M4.0 and M5.0 (Bommer and Crowley 2017). Table 2 indicates the seismicity parameters of all nine areal sources computed using the HA2 code.

4.2 Seismic hazard calculation

In order to compute ground motion intensity, seven GMPEs were selected (Zafarani and Farhadi 2017). Different characteristics of the selected GMPEs such as their applicable ranges of distance and magnitude are presented in Table 3. Moreover, Table 3 depicts specific site conditions employed for each GMPE to estimate the desired ground motion intensity. Considering the applicable period ranges of all implemented GMPEs, periods 0.01–3.0 s were selected to calculate the pseudo-spectral accelerations (PSA).

To perform the PSHA, the CRISIS2012 software (Ordaz et al. 2012) was used. Uniform hazard spectra (UHS) computed for 10% and 2% probability of exceedance in 50 years (i.e., the return periods of 475 and 2475 years, respectively) are shown in Fig. 11. Furthermore, Fig. 11 indicates a comparison between the UHS computed in the current study, standard design spectra for the site classes of I and II proposed by the Iranian seismic building code (BHRC14) for design with 10% probability of exceedance in 50 years, and the PSAs of east–west (H1) and north–south (H2) horizontal components of a recorded ground motion at the Sarpol-e Zahab station during the 2017 Sarpol-e Zahab earthquake ($M_w = 7.3$), Iran. The site was classified as I and II if the time-averaged shear wave velocity in the top 30 m of site is greater than 750 m/s, and ranged from 375 to 750 m/s, respectively. Figure 11 demonstrates that the 2475-year UHS (derived from the site conditions cited in Table 3) approximately mimics the general trend of the recorded SAs at all periods; however, they coincide better together at short periods of 0.01–0.4 s. Note that the recording station in the city was located on a rock site condition with $V_{s30} = 619$ m/s, close to the site condition values assumed in the UHS calculations (see Table 3). On the contrary, it should be highlighted that the BHRC14 standard design spectrum for site class of I matches the recorded SAs at the Sarpol-e Zahab station for the longer periods in the range of 0.4–3 s. The hazard
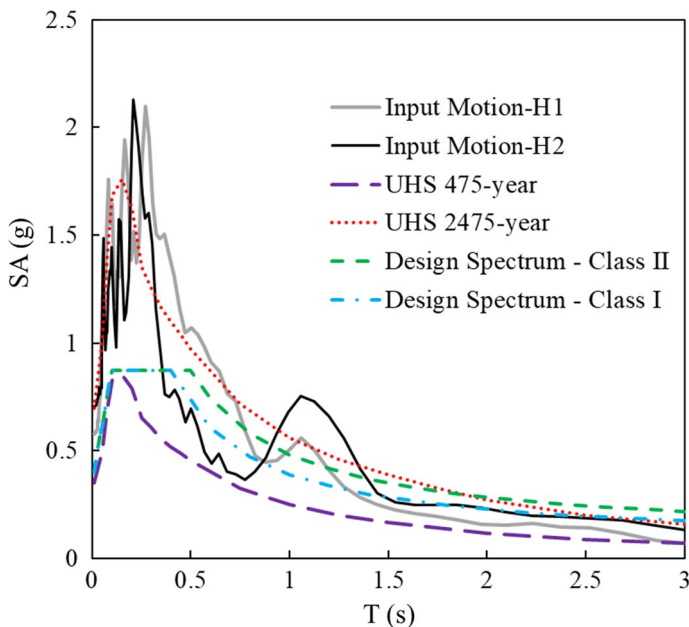

Fig. 11 Comparison between the computed uniform hazard, standard design (for different site classes), and the Sarpol-e Zahab recorded spectra
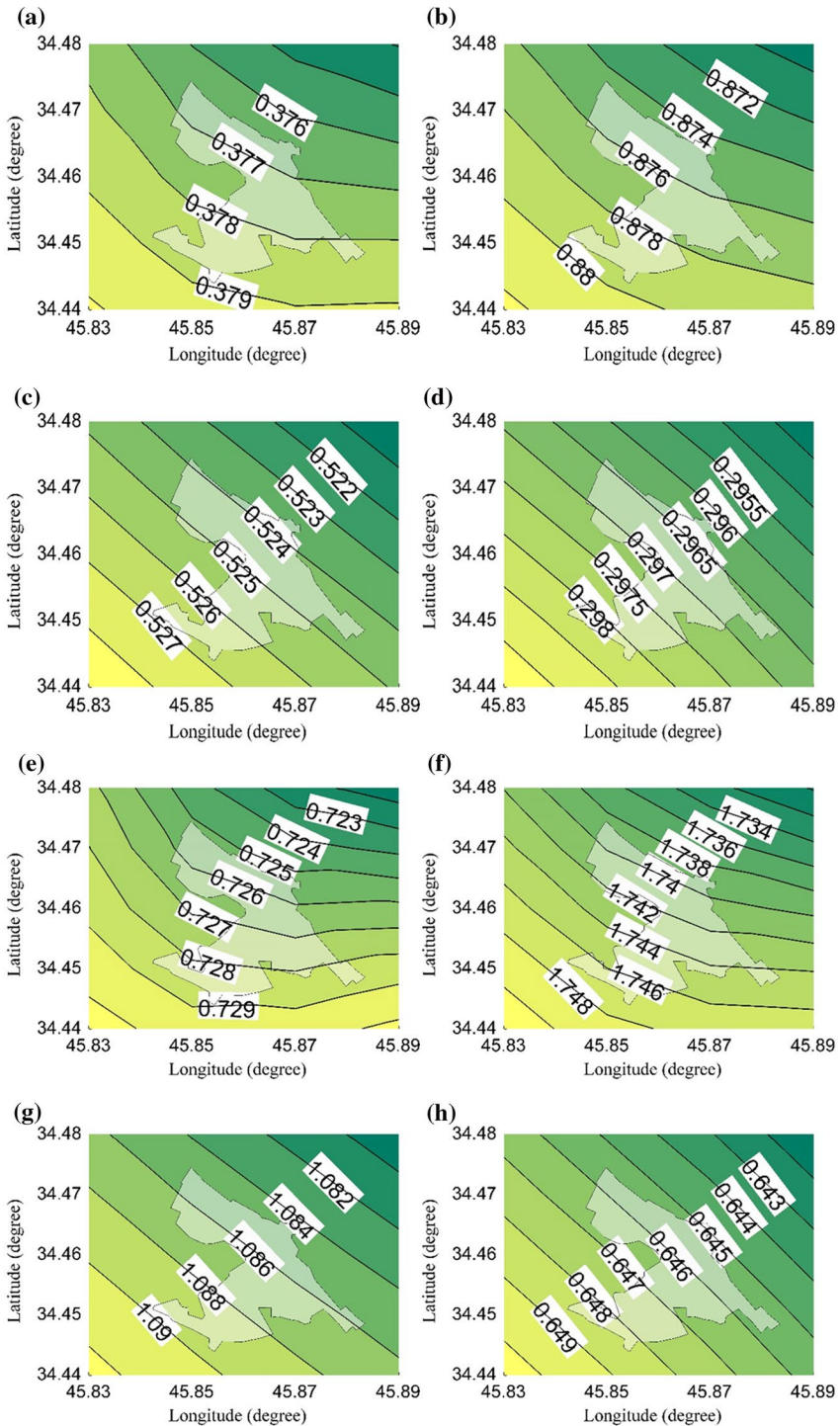
Fig. 12 The hazard map for Sarpol-e Zahab at return period of a 475 (**a–d**) and 2475 years (**e–h**) for the pseudo-spectral acceleration at oscillator periods of (**a, e**) 0.01 s (**b, f**) 0.20 s (**c, g**) 0.50 s (**d, h**) 1.00 s

map for the study region is also presented at four periods 0.01, 0.20, 0.50, and 1.00 s, for two return periods of 475 (Fig. 12a–d) and 2475 (Fig. 12e–g) years.

5 Local site effect

The earthquake site effects can significantly vary the seismic damages in the affected areas despite the closely equal source-to-site distances. The seismic response of a site depends on geotechnical, geometrical, and ground-motion parameters (e.g., Jafarian et al. 2018, 2019). Review of the available site conditions indicates that the Sarpol-e Zahab city has been built on highly variable geotechnical condition involving the deposits with various depths and properties. As shown in Fig. 3, the north of the city is surrounded by the Zagros Mountains, while the other side of the city (i.e., the Maskan-Mehr buildings) has been built near a river containing alluvium materials. Therefore, it seems that the damage pattern observed due to earthquake (see Fig. 3) is related to different site conditions, as discussed in the following sections.

6 Geological and geotechnical conditions

The geological map of the Sarpol-e Zahab region is shown in Fig. 13 which demonstrates that the city was constructed on two types of materials. The northern border of the city was formed by Asmari limestone where a rock outcrop can be observed. The eastern, western, and southern borders were located on a consolidated alluvium. The thickness of alluvial deposit varies from a few meters to several ten meters. The
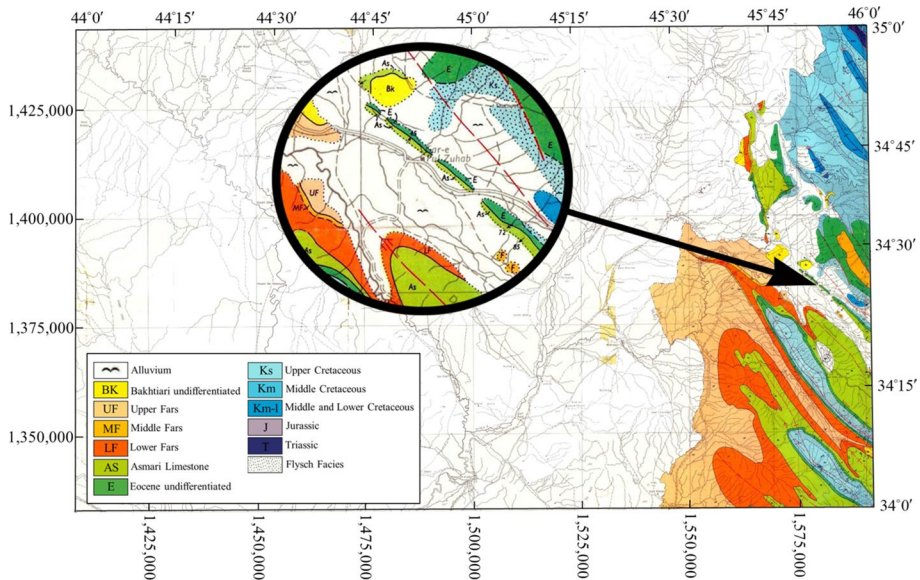

Fig. 13 Geological map of Sarpol-e Zahab (adapted from Iran National Cartographic Center, 1929)

thickness of alluvium increases across a river that passes from the southwest of Sarpol-e Zahab towards the north of this city.

To determine the ground-motion amplification, one must first estimate the geotechnical properties of the site. The geotechnical and geophysical data are not completely available for the all parts of the city. Nevertheless, seven geotechnical boreholes (BH) and one geophysical down-hole (DH) data were collected for Maskan-Mehr, the main site under consideration herein. Figure 14 shows the location of these boreholes along with the DH profile on the map. As seen in Fig. 14, the down-hole test was carried out about 500 m far away from the Maskan-Mehr buildings in the Fouladi neighborhood. Accordingly, the results of the down-hole test were also used for site response analyses of the Maskan-Mehr site. Figure 14 also illustrates location of the Sarpol-e Zahab recording station (SPZ).

Figure 15 illustrates the shear wave velocity (V_s) profile along with the characterization of the soil layers. The shear wave velocity was measured up to the depth of 30 m by a down-hole test at the DH point. The value is about 360 m/s at the depth of 30 m, while shear wave velocity in the top 30 m of the soil column (V_{s30}) at the SPZ station was measured to be equal to 619 m/s. A linear regression model was developed to estimate shear wave velocity, and then, an extrapolation was simply used to roughly estimate the depth of bedrock with $V_s = 619$ m/s as shown in Fig. 15. Accordingly, the depth of bedrock was estimated 46 m in the Maskan-Mehr site. The geotechnical boreholes indicate that the site of Maskan-Mehr involves a 10 m clay layer overlying a deep gravel layer. The average thickness of the clay layer was found by geotechnical data to be about 10 m. Some available correlations were used to determine the variations of shear modulus ratio (G/G_{max}) and damping (D) curves versus shear strain (γ). The curves of $G - \gamma$ and $D - \gamma$ are shown in Fig. 16 for clay (PI = 15) and gravel based on the models developed by Vucetic and Dobry(1991) and Kokusho (1980), respectively.
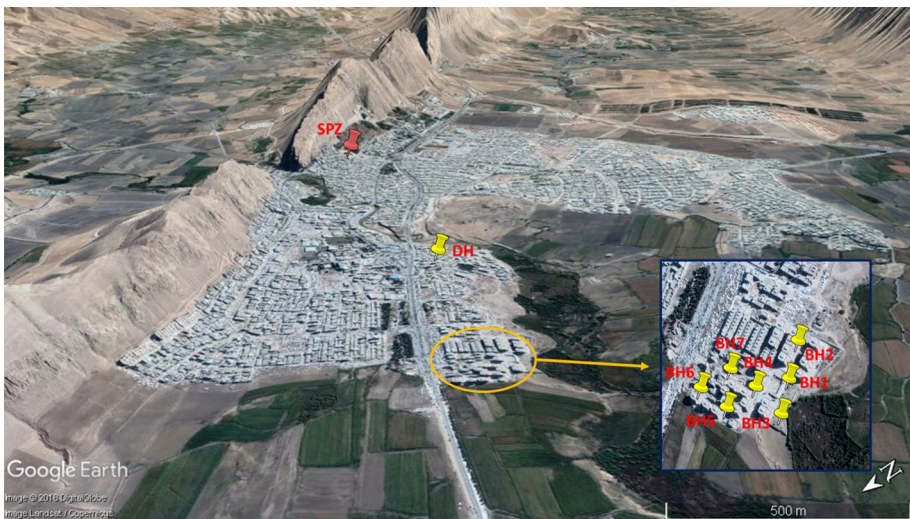

Fig. 14 Locations of geotechnical borehole site (BH), down-hole test site (DH), and the strong motion recording station (SPZ)
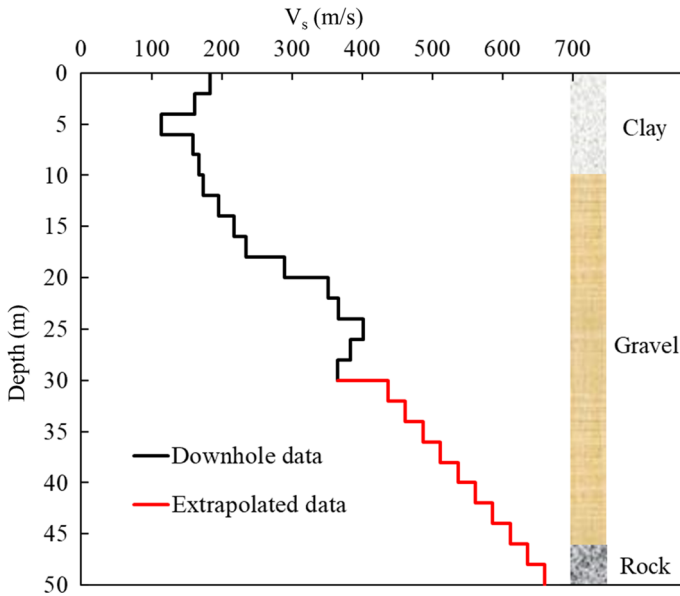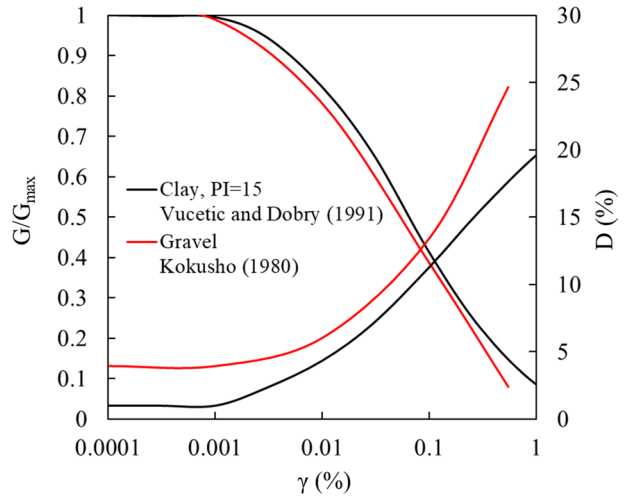
Fig. 15 The variations of shear wave velocity at the Maskan-Mehr site with depth

Fig. 16 Curves of shear modulus ratio and damping for clay and gravel utilized in this study

7 Site response analysis

One-dimensional site response analysis was performed based on the geotechnical and geophysical data of the Maskan-Mehr and the Fouladi neighborhood sites. The frequency-domain equivalent linear approach was employed to analyze the site response using DEEP-SOIL v.6 software (Hashash et al. 2016). The required soil properties such as shear wave velocity, shear modulus ratio, and damping curves were estimated as shown in Figs. 15–16. The recorded earthquake accelerations (including both horizontal components) in the SPZ

station were used as the input motions for the analyses. The model depth was determined by the extrapolation shown in Fig. 15 corresponding to the shear wave velocity of the recording station.

Figure 17 illustrates the acceleration response spectra of the input motion together with the surface motion resulted from the site response analysis. The comparison made between the input and the surface response spectra shows that the soil layers have filtered high frequency components of the input motion. Moreover, the bandwidth of the ground surface motion is considerably larger than that of the input wave. The period bound of the ground surface motion is about $T=0$–1.5 s for both the horizontal components, while it is about

Fig. 17 Comparison of acceleration response spectra of input motion, soil surface, and the BHRC14 design spectra for the horizontal components **a** east–west **b** north–south
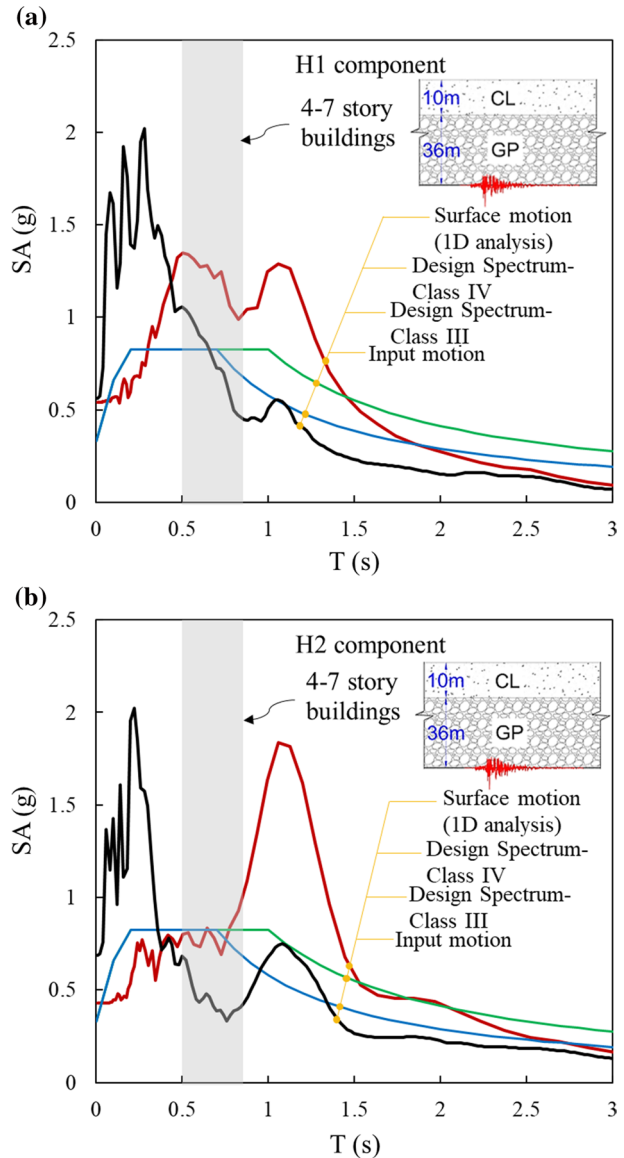
$T = 0$–0.5 s for the input motion. Figure 17 indicates that the predominant period is about $T = 0.5$ s and $T = 1$ s for surface response spectra of the east–west and north–south components, respectively. The predominant period of the input motion is about 0.4 s. The period of structures was estimated according to BHRC14 as follows:

$$T_s = 0.05H^{0.9} \tag{3}$$

where T_s is structure period in second and H is structure height in meters.

The period of structures is shown in Fig. 17 for the 4–7 stories buildings. The comparison between the surface response spectra and the range of structural periods indicates that the 4–7 stories buildings are potentially prone to response in resonance condition. As noted previously, the Maskan-Mehr buildings were 7-story RC building. Meanwhile, there are a few 4-story RC buildings that were completely destroyed under earthquake. Accordingly, it seems that the resonance phenomenon occurred in the site of Maskan-Mehr.

The design spectra of BHRC14 are plotted in Fig. 16 for soil types III ($175 < V_s < 375$ m/s) and IV ($V_s < 175$ m/s), where V_s stands for the averaged shear wave velocity of the upper 30 m of site. Based on the downhole data (see Fig. 15), the site of Maskan-Mehr is classified as type III ($V_{s30} = 217$ m/s). The BHRC14 design spectrum shows that the maximum SA is about 0.83 g for the 4–7 stories buildings. Figure 17a indicates that the maximum SA values of the east–west component for the 4 and 7 story buildings are about 1.35 g and 1.04 g, respectively. As seen in Fig. 17b, the maximum SA values of the north–south component for the same buildings are about 0.83 g and 1.09 g, respectively. Accordingly, the 4 and 7 stories buildings of the Maskan-Mehr site probably suffered accelerations of about 1.63 and 1.31 times the standard design acceleration during the earthquake, respectively.

As shown in Fig. 17, a 10-m-thick clay layer significantly affected the surface motion due to the proximity of the site fundamental period and earthquake motion predominant period. This phenomenon has been observed in previous earthquakes. For example, the 1985 Michoacan earthquake ($M_s = 8.1$) caused moderate and extensive damages in different areas of Mexico City. The structures located on the soft soil of the Lake Zone were suffered significant damage, while large parts of the city located on the dense soil experienced no damage (Kramer 1996). The previous studies (e.g., Seed et al. 1987) indicated that the natural period of the Mexico City clay was about 1.8–2 s. Accordingly, most buildings in the 5 to 20-story range suffered extensive damage due to the resonance phenomenon (Kramer 1996). This phenomenon was observed in Sarpol-e Zahab city where the buildings of Maskan-Mehr were located. The results of the downhole test indicate that the site of Maskan-Mehr is classified as type III based on BHRC14. Accordingly, the maximum site effect was considered for the design of the structures using BHRC14, while the 10-m clay layer probably created 1.63 times the standard design acceleration during the earthquake (See Fig. 17b).

8 Conclusion

This paper deals with the seismic hazard analysis and local site effect of Sarpol-e Zahab earthquake in Iran, occurred in November 2017 ($M_w = 7.3$). The reconnaissance investigations have shown that most of the earthquake losses occurred in the areas surrounding the Maskan-Mehr residential complex with 576 units which was built in 2012. Various

damages such as geotechnical and structural damages were observed throughout the Sarpol-e Zahab city.

The Sarpol-e Zahab earthquake was recorded by 109 free-field strong motion stations, whereas the maximum value of PGA was recorded at the Sarpol-e Zahab station at an epicentral distance of 35 km. The correction of strong motion records shows that the maximum PGA values of the recorded motion were about 0.69 g and 0.33 g for the horizontal and vertical components, respectively, in the Sarpol-e Zahab station with an epicentral distance of 35 km. The observed SA values in two stations were compared with predictions of five GMPEs.

The results of seismic hazard analysis indicated that the 2475-year UHS is in good agreement with both of the recorded SAs at approximately all periods; however, they coincide better together at the short periods of 0.01–0.4 s. On the contrary, the BHRC14 standard design spectrum for site class of I matches the recorded SAs at the Sarpol-e Zahab station for the long periods of 0.4–3 s. This means that the observed strong motions have return periods larger than 475 years and also, the Iranian seismic building code spectrum is not a uniform hazard spectrum and has different return periods at different oscillation periods.

One-dimensional equivalent linear analysis was used to evaluate the site response of the Maskan-Mehr site. The soil profile considered for the analyses changed the frequency content of motion, whereas it magnified the low-frequency components of the motion. The results also indicate that the 4–7 stories building around this site probably suffered a resonance condition. The maximum SA values of the east–west and north–south components are about 1.35 g and 1.09 g for the 4 and 7 stories buildings, respectively. Accordingly, the 4 and 7 stories buildings of the Maskan-Mehr site probably suffered accelerations of about 1.63 and 1.31 times the standard design acceleration during the earthquake, respectively.

References

Abrahamson NA, Silva WJ, Kamai R (2014) Summary of the ASK14 ground motion relation for active crustal regions. Earthq Spectra 30(3):1025–1055

Ambraseys NN, Melville CP (2005) A history of Persian earthquakes. Cambridge University Press, Cambridge

Ansari A, Noorzad A, Zafarani H, Vahidifard H (2010) Correction of highly noisy strong motion records using a modified wavelet de-noising method. Soil Dyn Earthq Eng 30:1168–1181

Berberian M (1994) Natural hazards and the first earthquake catalogue of Iran. International Institute of Earthquake Engineers and Seismology, Tehran

Bommer JJ, Crowley H (2017) The purpose and definition of the minimum magnitude limit in PSHA calculations. Seismol Res Lett 88:1097–1106

Bommer JJ, Douglas J, Scherbaum F, Cotton F, Bungum H, Fäh D (2010) On the selection of ground-motion prediction equations for seismic hazard analysis. Seismol Res Lett 81:783–793

Boore DM, Stewart JP, Seyhan E, Atkinson GM (2014) NGA-West2 equations for predicting PGA, PGV, and 5% damped PSA for shallow crustal earthquakes. Earthq Spectra 30:1057–1085

Building and Housing Research Center (BHRC) (2014) Iranian code of practice for seismic resistant design of buildings (standard no. 2800). Building and Housing Research Center Tehran, Iran.

Campbell KW, Bozorgnia Y (2014) NGA-West2 ground motion model for the average horizontal components of PGA, PGV, and 5% damped linear acceleration response spectra. Earthq Spectra 30:1087–1115

Chiou BS-J, Youngs RR (2014) Update of the Chiou and Youngs NGA ground motion model for average horizontal component of peak ground motion and response spectra. Earthq Spectra 30:1117–1153

Danciu L, Şeşetyan K, Demircioglu M, Gülen L, Zare M, Basili R, Elias A, Adamia S, Tsereteli N, Yalçın H, Utkucu M, Khan MA, Sayab M, Hessami K, Rovida AN, Stucchi M, Burg J-P, Karakhanian A, Babayan H, Avanesyan M, Mammadli T, Al-Qaryouti M, Kalafat D, Varazanashvili O, Erdik M, Giardini D (2018) The 2014 earthquake model of the Middle East: seismogenic sources. Bull Earthq Eng 16:3465–3496. https://doi.org/10.1007/s10518-017-0096-8

Farzanegan ES, Pourmohammad Shahvar M, Eshaghi A, Mirsanjari M, Abdollahi H, Mirzaee Alavijeh H (2017) Report of the November 12, 2017 Sarpol-e Zahab, Kermanshah Province earthquake

Gardner J, Knopoff L (1974) Is the sequence of earthquakes in Southern California, with aftershocks removed, Poissonian? Bull Seismol Soc Am 64:1363–1367

Hashash Y, Musgrove M, Harmon J, Groholski D, Phillips C, Park D (2016) DEEPSOIL 6.1, user manual. Urbana, IL, Board of Trustees of University of Illinois at Urbana-Champaign

Idriss I (2008) An NGA empirical model for estimating the horizontal spectral values generated by shallow crustal earthquakes. Earthq Spectra 24:217–242

Iran National Cartographic Center (1929) Qasr-e-Shirin. Iran 1:250,000 scale geological maps

Jafarian Y, Lashgari A, Miraei M (2018) Multivariate fragility functions for seismic landslide hazard assessment. J Earthq Eng. https://doi.org/10.1080/13632469.2018.1528909

Jafarian Y, Lashgari A, Haddad A (2019) Predictive Model and probabilistic assessment of sliding displacement for regional scale seismic landslide hazard estimation in Iran. Bull Seismol Soc Am 109:1581–1593. https://doi.org/10.1785/0120190004

Kale Ö, Akkar S, Ansari A, Hamzehloo H (2015) A ground-motion predictive model for Iran and Turkey for horizontal PGA, PGV, and 5% damped response spectrum: investigation of possible regional effects. Bull Seismol Soc Am 105:963–980

Kanno T, Narita A, Morikawa N, Fujiwara H, Fukushima Y (2006) A new attenuation relation for strong ground motion in Japan based on recorded data. Bull Seismol Soc Am 96:879–897

Khodaverdian A, Zafarani H, Rahimian M, Dehnamaki V (2016) Seismicity parameters and spatially smoothed seismicity model for Iran. Bull Seismol Soc Am 106:1133–1150

Kijko A (2004) Estimation of the maximum earthquake magnitude, m max. Pure Appl Geophys 161:1655–1681

Kijko A (2010) Seismic hazard assessment for selected area. Description of MATLAB Code, HA2, **2**.

Kijko A, Sellevoll M (1989) Estimation of earthquake hazard parameters from incomplete data files. Part I. Utilization of extreme and complete catalogs with different threshold magnitudes. Bull Seismol Soc Am 79:645–654

Kijko A, Sellevoll MA (1992) Estimation of earthquake hazard parameters from incomplete data files. Part II. incorporation of magnitude heterogeneity. Bull Seismol Soc Am 82:120–134

Kokusho T (1980) Cyclic triaxial test of dynamic soil properties for wide strain range. Soils Found 20:45–60

Kramer S (1996) Geotechnical earthquake engineering. Prentice-Hall, Inc., New Jersey, pp 348–422

Mirzaei N, Mengtan G, Yuntai C (1998) Seismic source regionalization for seismic zoning of Iran: major seismotectonic provinces. J Earthq Predict Res 7:465–495

Onur T, Gök R, Abdulnaby W, Mahdi H, Numan NM, Al-Shukri H, Shakir AM, Chlaib HK, Ameen TH, Abd NA (2017) A comprehensive earthquake catalog for Iraq in terms of moment magnitude. Seismol Res Lett 88:798–811

Ordaz M, Martinelli F, Aguilar A, Arboleda J, Meletti C, D'amico, V. (2012) Program for computing seismic hazard (CRISIS 2012). Instituto de Ingeniería, Universidad Nacional Autónoma de México (UNAM), Mexico Google Scholar, Mexico

Seed HB, Romo M, Sun J, Jaime A, Lysmer J (1987) Relationships between soil conditions and earthquake ground motions in Mexico City in the earthquake of Sept 19, 1985. Earthquake Engineering Research Center, University of California, Berkeley, EERC, Report UCB/EERC-87/15

Shahvar MP, Zare M, Castellaro S (2013) A unified seismic catalog for the Iranian plateau (1900–2011). Seismol Res Lett 84:233–249

Vucetic M, Dobry R (1991) Effect of soil plasticity on cyclic response. J Geotech Eng 117:89–107

Zafarani H, Farhadi A (2017) Testing ground-motion prediction equations against small-to-moderate magnitude data in Iran. Bull Seismol Soc Am 107(2):912–933

Zafarani H, Soghrat M (2012) Simulation of ground motion in the Zagros region of Iran using the specific barrier model and the stochastic method. Bull Seismol Soc Am 102:2031–2045

Zafarani H, Soghrat M (2017) A selected dataset of the Iranian strong motion records. Nat Hazards 86:1307–1332

Zafarani H, Luzi L, Lanzano G, Soghrat M (2018) Empirical equations for the prediction of PGA and pseudo spectral accelerations using Iranian strong-motion data. J Seismolog 22:263–285

Zare M, Amini H, Yazdi P, Sesetyan K, Demircioglu MB, Kalafat D, Erdik M, Giardini D, Khan MA, Tsereteli N (2014) Recent developments of the Middle East catalog. J Seismolog 18:749–772

Zhao JX, Zhang J, Asano A, Ohno Y, Oouchi T, Takahashi T, Ogawa H, Irikura K, Thio HK, Somerville PG (2006) Attenuation relations of strong ground motion in Japan using site classification based on predominant period. Bull Seismol Soc Am 96:898–913

Affiliations

Hamid Zafarani[1] · Yaser Jafarian[1] · Alireza Eskandarinejad[2] · Ali Lashgari[3] · Mohammad Reza Soghrat[1] · Hassan Sharafi[4] · Masoud Afraz-e Haji-Saraei[5]

Hamid Zafarani
h.zafarani@iiees.ac.ir

Alireza Eskandarinejad
a.eskandarinejad@gu.ac.ir

Ali Lashgari
ali.lashgarii@semnan.ac.ir

Mohammad Reza Soghrat
mr.soghrat@gmail.com

Hassan Sharafi
h_sharafi@razi.ac.ir

Masoud Afraz-e Haji-Saraei
sigordevar@yahoo.com

[1]   International Institute of Earthquake Engineering and Seismology, Tehran, Iran

[2]   Department of Civil Engineering, Faculty of Engineering, Golestan University, Gorgan, Iran

[3]   Department of Civil Engineering, Semnan University, Semnan, Iran

[4]   Civil Engineering Department, Razi University, Kermanshah, Iran

[5]   Office of National Regulations and Building Control, Tehran, Iran